iScience

CellPress
OPEN ACCESS

Article

Understanding oxygen evolution mechanisms by tracking charge flow at the atomic level

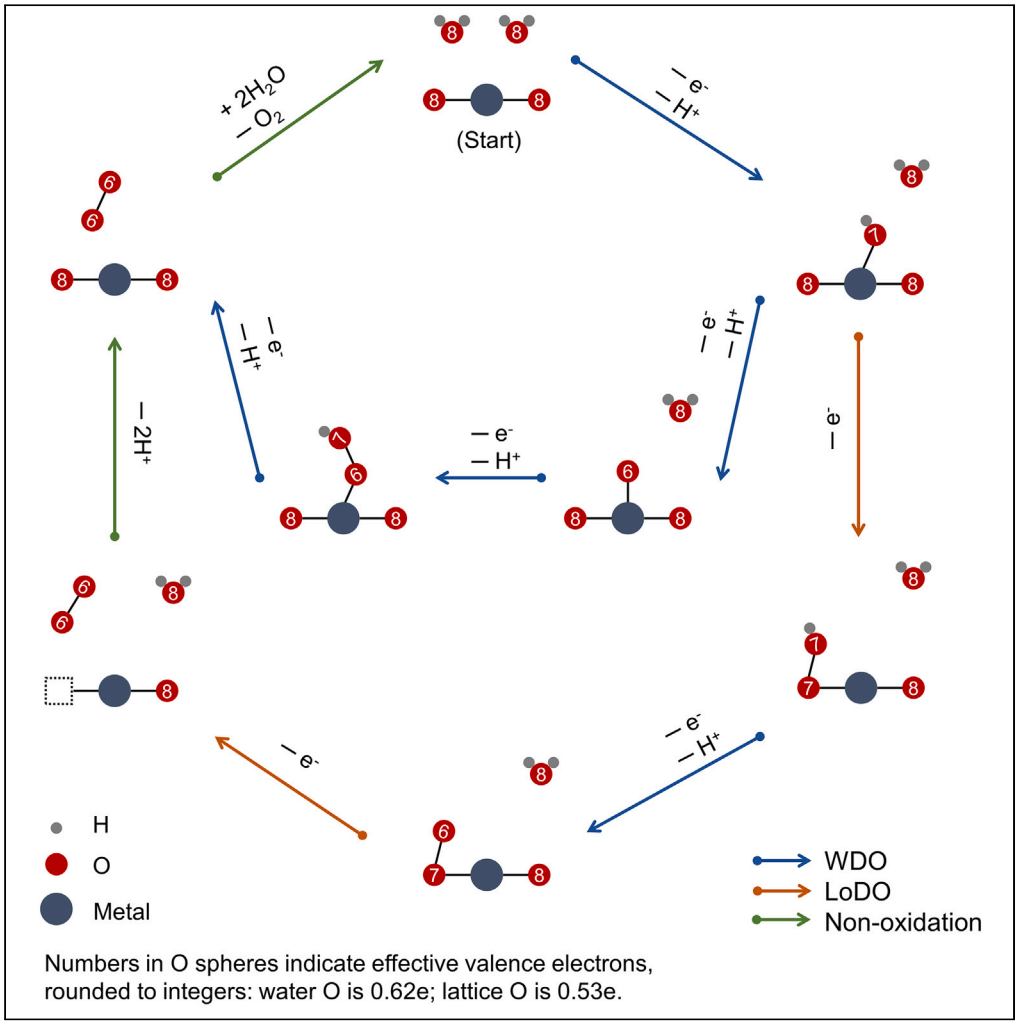

Numbers in O spheres indicate effective valence electrons, rounded to integers: water O is 0.62e; lattice O is 0.53e.

Changming Zhao, Hao Tian, Zhigang Zou, Hu Xu, Shuk-Yin Tong

xuh@sustech.edu.cn (H.X.)
tongsy@cuhk.edu.cn (S.-Y.T.)

Highlights

One cannot classify OER catalysts without considering the energy levels of water

For metal-oxide catalysts, each e removal step may be either WDO, LoDO, or MDO

Charge is mainly taken from water levels in AEM, not from the anchoring metal atoms

Catalysts with oxygen bands above metal bands, OER may be WDO or mixed WDO and LoDO

Zhao et al., iScience 26, 107037
July 21, 2023 © 2023
https://doi.org/10.1016/j.isci.2023.107037

iScience

CellPress
OPEN ACCESS

Article

Understanding oxygen evolution mechanisms by tracking charge flow at the atomic level

Changming Zhao,[1,2,5] Hao Tian,[1,3,5] Zhigang Zou,[1] Hu Xu,[2,*] and Shuk-Yin Tong[1,2,4,5,6,*]

SUMMARY

Current classifications of oxygen evolution catalysts are based on energy levels of the clean catalysts. It is generally asserted that a LOM-catalyst can only follow LOM chemistry in each electron transfer step and that there can be no mixing between AEM and LOM steps without an external trigger. We use *ab initio* theory to track the charge flow of the water-on-catalyst system and show that the position of water orbitals is pivotal in determining whether an electron transfer step is water dominated oxidation (WDO), lattice-oxygen dominated oxidation (LoDO), or metal dominated oxidation (MDO). Microscopic photo-catalytic pathways of TiO_2 (110), a material whose lattice oxygen bands lie above the metal bands, show that viable OER pathways follow either all AEM steps or mixed AEM-LOM steps. The results provide a correct description of redox chemistries at the atomic level and advance our understanding of how water-splitting catalysts produce desorbed oxygen.

INTRODUCTION

Understanding the oxygen evolution mechanism is crucial to rational design of active catalysts that can split water efficiently to obtain green hydrogen fuel. Two milestones have been achieved in more than a decade of research. The first milestone is reached by Nørskov et al.[1,2] who established that oxygen evolution reaction (OER) involves removing four electrons from a water-on-catalyst system. The electron removal may be achieved by action of photo-holes (as in photocatalysis of water) or by an external battery connected to the system with a proper voltage (as in electrolysis of water). After four electrons are removed, an oxygen molecule desorbs from the surface. The early works of Nørskov et al. mainly focused on rutile oxides[2,3] and perovskites[4] where the desorbed oxygen molecule is made up of O_{w1}-O_{w2}. Here, O_{w1} and O_{w2} denote the oxygen atoms from the first and second water respectively. A second milestone was reached recently when anionic activity of lattice oxygen was proposed with experimental observations and theoretical explanations.[5–7] Grimaud et al.[8] further used oxide catalysts with O_{18} isotopes and detected lattice oxygen in the desorbed oxygen molecule (i.e., O_{w1}-$O_{lattice}$). Since then, numerous works have focused on finding OER mechanisms at the atomic level[9–12] to explain the measured catalytic performance of different catalysts.[13–15] Although OER pathways at the microscopic level with reaction barriers of intermediates, etc., are still largely missing, there seems to be general consensus on a few points. The first general view is that OER pathways follow one of two routes: either an adsorbate evolution mechanism (AEM) or a lattice oxygen mechanism (LOM).[9,11] The second view is that a metal-oxide catalyst can be classified according to whether its metal bands are above (i.e., nearer to the Fermi level) or below its lattice oxygen bands. If the metal bands are above, then the catalyst is classified as an AEM-catalyst. Conversely, if lattice oxygen bands are above, then the catalyst is a LOM-catalyst.[6,16] A third generally accepted view is that an AEM-catalyst can only follow the AEM route in each of its four electron transfer steps, whereas a LOM-catalyst can only follow the LOM route in each of its four electron transfer steps. There can be no mixing between AEM and LOM steps without the action of an external trigger.[16]

In this work, we investigate the validity of the above views using *ab initio* theory. Our calculations differ from previous studies in a number of aspects. The Hamiltonian used is the spin-polarized density functional theory with HSE06 hybrid functionals.[17,18] This Hamiltonian provides more accurate electronic levels than ordinary (semi)-local DFT functionals employed in previous studies.[19–22] Partial density of states (PDOS) provides information of water, lattice oxygen and metal derived orbitals relative to the Fermi level. However, PDOS does not inform how much charge is removed from a particular atom because: (1) PDOS is information in reciprocal space, and (2) the sum of PDOS does not add up to the total DOS of the system. To

[1]School of Science and Engineering, The Chinese University of Hong Kong, Shenzhen 518172, China

[2]Department of Physics, Southern University of Science and Technology, Shenzhen 518055, China

[3]University of Science and Technology of China, Chemistry and Material Science College, Hefei 230026, China

[4]Institute of Materials Science and Devices, Suzhou University of Science and Technology, Suzhou 215009, China

[5]These authors contributed equally

[6]Lead contact

*Correspondence: xuh@sustech.edu.cn (H.X.), tongsy@cuhk.edu.cn (S.-Y.T.)

https://doi.org/10.1016/j.isci.2023.107037

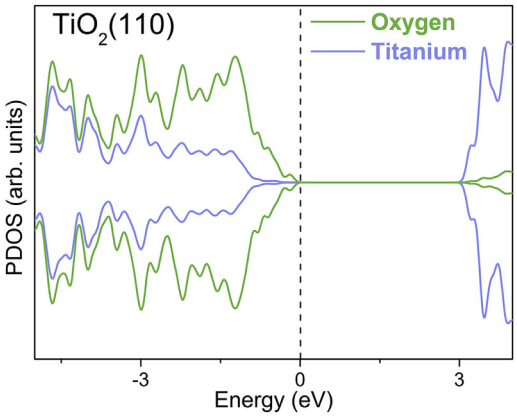

Figure 1. PDOS of TiO_2 (110) slab
The vertical dotted line marks the Fermi level. The PDOS is dominated by lattice oxygen orbitals, making TiO_2 a LOM-catalyst.

determine quantitatively how much charge is removed from each atom, we use the Bader charge method.[23,24] The detailed movement of charge taken from or given to each atom at each step is extremely important to differentiating between AEM and LOM steps. To our knowledge, no previous work has presented Bader analyses to track down the source of charge transfers, to determine how much charge is taken from water, lattice oxygen or metal atoms respectively.

For illustration, we show OER of photocatalysis on rutile TiO_2. Rutile TiO_2 is the benchmark catalyst used to demonstrate fundamental processes of photocatalysis because it is abundant, inert, non-toxic and photostable.[25] On TiO_2 (110), the electronic states at (near) the Fermi level are dominated by lattice oxygen orbitals.[26] Thus, it is a LOM-catalyst according to consensus two.[6,16] Figure 1 shows its PDOS near the Fermi level. We choose two well-established pathways: the first is the one proposed by Nørskov et al.,[1,2,4] whereas the second pathway is proposed by Wang et al.[27] The results and implications differ substantially from the current viewpoints. They are presented in the next section. Discussions then follow.

RESULTS

Pathway 1: A LOM-catalyst with four AEM steps

Photocatalysis of water on TiO_2 (110) starts with an initial state (IS) comprising the TiO_2 (110) slab and two unattached water molecules in the ambient (see Computational Method). The first water adsorbs at an on-top Ti surface site (a 5-fold coordination site Ti_5) and the adsorption is slightly exothermic. The first photohole arrives and removes an electron from the system and sheds a proton from the adsorbed water, forming structure S1. A second hole arrives and removes a second electron and sheds a second proton to form structure S2. The second free water adsorbs at a neighboring Ti_5 site. A third hole arrives and removes a third electron and sheds a proton from the second water, leaving an O_{w2}-H dimer on the neighboring Ti_5. The dimer hops to form a Ti_5-O_{w1}-O_{w2}-H chain (structure S3). A fourth hole arrives to remove a fourth electron and shed the proton from the chain. An oxygen molecule, comprising O_{w1}-O_{w2}, desorbs from the system and the final state (FS) is arrived. The four electron transfer steps can be represented by the following four equations:

$$1)\ * + H_2O \rightarrow *OH + H^+ + e^-$$

$$2)\ *OH \rightarrow *O + H^+ + e^-$$

$$3)\ *O + H_2O \rightarrow *OOH + H^+ + e^-$$

$$4)\ *OOH \rightarrow * + O_2 + H^+ + e^-$$

Two new water molecules from the ambient arrive and the process repeats, releasing more O_{w1}-O_{w2} molecules. The four electron removal steps and intermediates formed are shown schematically in Figure 2, upper panel.

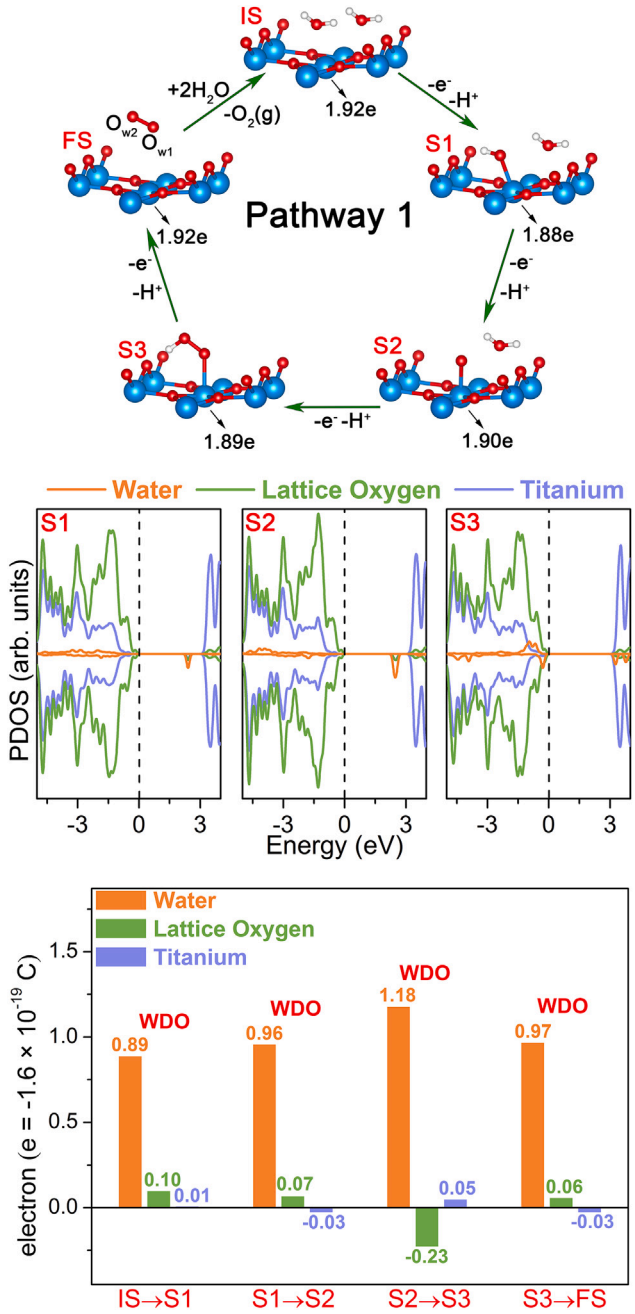

Figure 2. Pathway 1

Upper panel: Schematic diagrams with metal: blue, oxygen: red, hydrogen: white. Middle panel: PDOS of adsorbed water, lattice oxygen and metal for structures S1, S2 and S3. The vertical dotted line marks the Fermi level. Because at most only two water molecules are adsorbed, for easier visualization of the water PDOS, the metal and lattice oxygen PDOS include only 16 Ti and 32 lattice oxygen atoms in the "top layer". However, the full slab is used everywhere else, in calculations of Bader charge, etc. Lower panel: Bader analysis of net charge, in units of e = -1.6×10^{-19} C, collectively taken from or taken by water, lattice oxygen or metal atoms by action of each photo-hole. The charge at the Ti_5 site where the surface chain is anchored is indicated in the upper panel schematic diagram for states IS, S1, S2, S3 and FS. It is worth noting that the charge fluctuation is of the order 0.04e or less.

Pathway 1 essentially follows the four-step process outlined by Nørskov et al.[1,2,4] where each of the four photo-holes removes an electron with charge e = -1.6×10^{-19} C from the system. At the time of each electron removal, a proton is released, in a concerted electron-proton transfer (CEPT) process.[28,29] We show in Figure 2, middle panel, the PDOS of water, lattice oxygen and metal for structures S1, S2 and S3. Although PDOS diagrams show substantial presence of water and lattice oxygen orbitals at (near) the Fermi level, the reciprocal space distributions do not provide information on charge movement at individual atoms in the system. Bader analysis provides such real space information and the results are shown in the lower panel of Figure 2 (see also Computational Method and Supplementary Information). For example, the first photo-hole takes a total of 0.89e from the first water molecule and very small amounts (a net total of 0.1e and 0.01e) respectively from lattice oxygen and metal atoms in the catalyst. Similar charge analyses from each of the three sources-water, lattice oxygen and metal atoms-are shown for the subsequent three electron transfers in Figure 2 lower panel. Because of orbital hybridization, the charge comes from many atoms of each source. For each step, water, lattice oxygen, or metal atoms may experience a net outflow (oxidation) or inflow (reduction) of electrons. Collectively, the two water molecules are oxidized at each of the four steps; lattice oxygen atoms are collectively oxidized at steps 1, 2 and 4, reduced at step 3; whereas metal atoms are collectively oxidized at steps 1 and 3, reduced at steps 2 and 4. The order of redox depends sensitively on the structure and composition of the intermediates. After the four steps, the two water experience a net outflow of 4e, whereas both lattice oxygen and metal atoms experience zero charge change. If we define an electron removal step as either being water-dominated oxidation (WDO), lattice-oxygen dominated oxidation (LoDO) or metal-dominated oxidation (MDO), depending on from which source the majority of charge is removed, then pathway 1 is made up of four WDO steps. According to the consensus viewpoint, pathway 1 should be classified as adsorbate evolution mechanism (AEM)[3,8,16] because all four electrons are removed from water (adsorbate) and none from lattice oxygen or metal atoms. However, TiO_2 is a LOM-catalyst according to current viewpoint[9,16] and this creates a contradiction. Therefore, the current viewpoint needs revision. We shall provide suggestions to fix the contradiction in the Discussion section.

Pathway 2: A LOM-catalyst with mixed AEM and LOM steps

The second pathway, first suggested by Wang et al.,[27] starts with the same initial state (IS) and structure S1 of pathway 1. Then, the O_{w1}-H dimer on Ti_5 moves to interact with a nearby bridge oxygen (O_{br}) and when a second photo-hole arrives to remove an electron from the system, a $(Ti_6)_2$-O_{br}-O_{w1}-H chain is formed (structure S4, Figure 3). A third hole arrives, removes an electron and sheds the chain of its proton. This results in the upright $(Ti_6)_2$-O_{br}-O_{w1} structure of S5. A fourth hole arrives to remove an electron and an oxygen molecule, comprising a lattice oxygen and a water oxygen, desorbs from the surface, thereby creating a vacancy at the bridge site (S6). A second water fills the vacancy and the oxygen of the second water forms bonds with Ti_6 and releases its two protons. After shedding two protons, the final state (FS) is reached, except now, the oxygen of the second water has replaced the desorbed lattice O_{br}. Two new water molecules arrive and the OER process repeats. The four electron transfer steps can be represented by the following four equations (here, *(O_{br}) means that the OH adsorbs at a bridge oxygen site, and *(Vac) means that the slab has a vacancy at a bridge oxygen site):

$$5)\ * + H_2O \rightarrow *OH + H^+ + e^-$$

$$6)\ *OH \rightarrow *(O_{br})OH + e^-$$

$$7)\ *(O_{br})OH \rightarrow *(O_{br})O + H^+ + e^-$$

$$8)\ *(O_{br})O \rightarrow *(Vac) + O_2 + e^-$$

$$9)\ *(Vac) + H_2O \rightarrow * + 2H^+$$

Again, we turn to Bader analysis for real space information on charge movements (lower panel, Figure 3). As in pathway 1, the first photo-hole takes 0.89e from the first water molecule and a net of 0.1e, 0.01e respectively from lattice oxygen and metal atoms. The second photo-hole takes a net of 0.67e from lattice oxygen atoms, and lesser amounts 0.17e and 0.16e respectively from water and metal atoms. Thus, this step is lattice oxygen dominated oxidation (LoDO). The third photo-hole takes 0.87e from the first water molecule

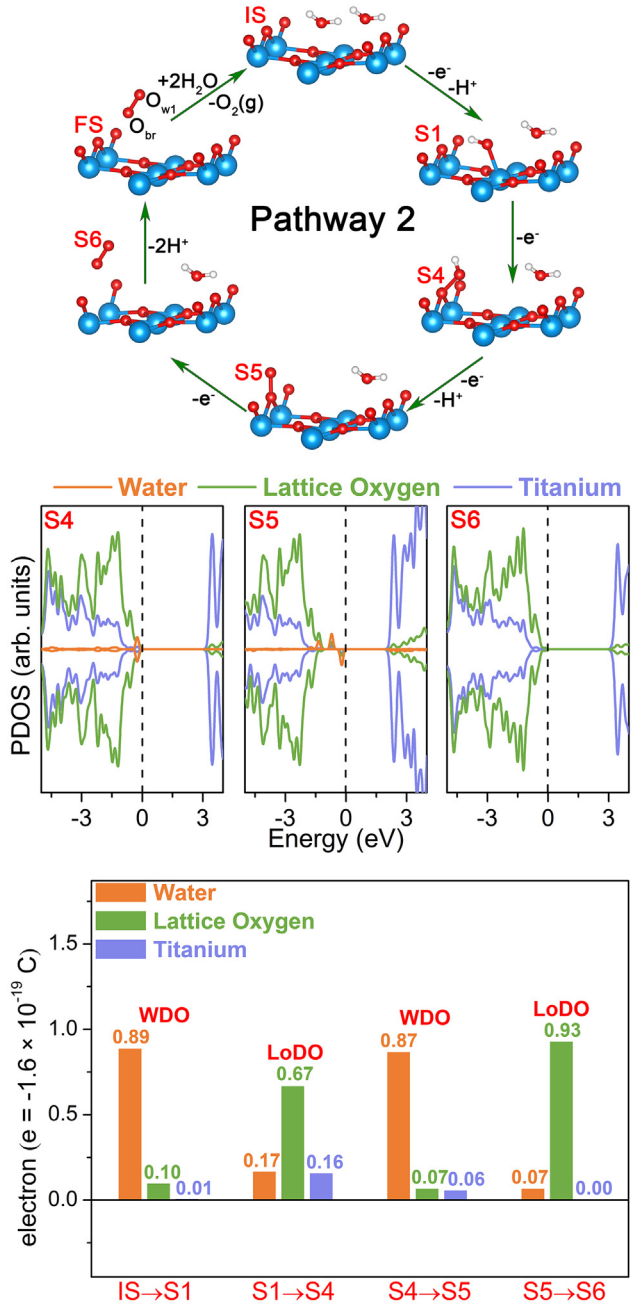

Figure 3. Pathway 2

Upper panel: Schematic diagrams with metal: blue, oxygen: red, hydrogen: white. Middle panel: PDOS of adsorbed water, lattice oxygen and metal for structures S4, S5 and S6. The vertical dotted line marks the Fermi level. Because only one water molecule is adsorbed, for easier visualization of the water PDOS, the metal and lattice oxygen PDOS include only 16 Ti and 32 lattice oxygen atoms in the "top layer". However, the full slab is used everywhere else, in calculations of Bader charge, etc. Lower panel: Bader analysis of net charge, in units of e = -1.6×10^{-19} C, collectively taken from or taken by water, lattice oxygen or metal atoms by action of each photo-hole.

and a net of 0.07e, 0.06e respectively from lattice oxygen and metal atoms. This is a WDO step. The fourth photo-hole takes a net of 0.93e from lattice oxygen atoms, 0.07e from the first water and no charge from metal atoms. This step is LoDO. After four photo-holes, an aggregate of 2.0e is taken from the first water molecule, 1.77e from lattice oxygen atoms and 0.23e from metal atoms. The O_{br} atom connected to O_{w1}

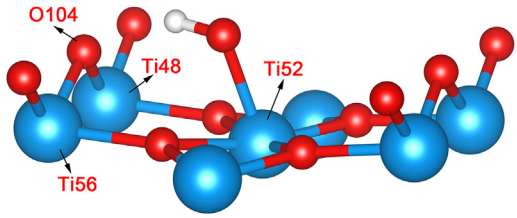

Figure 4. Schematic diagram of the S1 state, some atoms are identified with numbers
Blue: Ti, red: oxygen, white: hydrogen.

has 6e remaining, so does the O_{w1} atom. The pair desorb from the lattice, leaving a vacancy. A second water fills the vacancy, with O_{w2} carrying 6.93e to fill the vacancy and become a new bridge atom. The second water also gives 0.84e to the rest of the lattice oxygen atoms and 0.23e to the metal atoms. With that, the charge in the catalyst is restored. In this pathway, water, lattice oxygen and metal atoms are collectively oxidized at each step. The pathway switches between WDO and LoDO steps, following WDO, LoDO, WDO and LoDO.

In Figure 4, we show a schematic diagram of state S1 with numbers identifying the atoms shown in the supplementary information.

DISCUSSION

To better understand redox mechanisms in OER pathways, it is essential to gain charge flow information at the atomic level. From our analysis, we make the following observations and suggestions.

1) For metal-oxide catalysts, each e removal may be either water dominated (WDO), lattice oxygen dominated (LoDO), or metal dominated (MDO), depending on which of the three sources is most oxidized.
2) For good OER catalysts, water should occur as a lightly adsorbed surface impurity.[30] Thus, the water-derived orbitals would occupy energy levels at (near) the Fermi level. For metal-oxide catalysts whose lattice oxygen bands are substantially above the metal bands, the levels at (near) the Fermi level would be either water dominated or water-and-lattice-oxygen co-dominated. In the former case, the four steps of OER would follow WDO. In the latter case, the four steps may be either entirely WDO or a mixture of WDO and LoDO, depending on the intermediates formed.
3) For metal-oxide catalysts whose metal bands are substantially above the lattice oxygen bands, the levels at (near) the Fermi level would be water dominated or water-and-metal co-dominated. In the former case, the four steps of OER would follow WDO. In the latter case, the four steps would be either entirely WDO or a mixture of WDO and MDO. However, catalysts that follow MDO steps are rare and tend to be unstable because strong metal oxidation would lead to dissolution of the catalyst.
4) It is inappropriate to classify clean catalysts without considering the energy levels of water-derived orbitals.

In the literature, we find many schematic diagrams of OER pathways where the metal atoms take in or give out more than one electronic charge.[6,8,16] Such redox processes are impossible for catalysts whose metal bands are below the oxygen bands. An example is TiO_2, where charge flow into or out of metal atoms is minimal at all steps for either pathway 1 or 2. Bader charge analysis provides real space charge flow information. Its use reveals precise information of redox effects. This information greatly aids the design of better water splitting catalysts. We suggest that any schematic diagram of pathway steps should be accompanied by Bader charge analysis, to lend credibility to the charge flow charts.

Limitations of the study

The charge on each atom of the intermediates is calculated by *ab initio* theory for the four steps in photocatalysis. The zero-order assumption is that the charge on similar intermediates of electrocatalysis is the same.

STAR★METHODS

Detailed methods are provided in the online version of this paper and include the following:

- KEY RESOURCES TABLE
- RESOURCE AVAILABILITY
  - Lead contact
  - Materials availability
  - Data and code availability
- METHOD DETAILS

SUPPLEMENTAL INFORMATION

Supplemental information can be found online at https://doi.org/10.1016/j.isci.2023.107037.

ACKNOWLEDGMENTS

This work is supported by the National Natural Science Foundation of China (Grant No. 11974160 and 12174326), Science, Technology and Innovation Commission of Shenzhen Municipality (Grant No. RCYX20200714114523069), Guangdong Introducing Innovative and Entrepreneurial Teams (Grant No. 2019ZT08L101), Shenzhen Natural Science Foundation (Grant No. GXWD20201231105722002-20200824163747001), Shenzhen Key Laboratory of Eco-materials and Renewable Energy (Grant No. ZDSYS20200922160400001). We would like to thank Center for Computational Science and Engineering at Southern University of Science and Technology for providing computing resources.

AUTHOR CONTRIBUTIONS

The manuscript was written through contributions of all authors. All authors have given approval to the final version of the manuscript.

DECLARATION OF INTERESTS

The authors declare no conflict of interest.

INCLUSION AND DIVERSITY

We support inclusive, diverse, and equitable conduct of research.

Received: February 21, 2023
Revised: March 22, 2023
Accepted: June 1, 2023
Published: June 8, 2023

REFERENCES

1. Nørskov, J.K., Rossmeisl, J., Logadottir, A., Lindqvist, L., Kitchin, J.R., Bligaard, T., and Jónsson, H. (2004). Origin of the overpotential for oxygen reduction at a fuel-cell cathode. J. Phys. Chem. B *108*, 17886–17892. https://doi.org/10.1021/jp047349j.

2. Valdés, Á., Qu, Z.W., Kroes, G.J., Rossmeisl, J., and Nørskov, J.K. (2008). Oxidation and photo-oxidation of water on TiO_2 surface. J. Phys. Chem. C *112*, 9872–9879. https://doi.org/10.1021/jp711929d.

3. Rossmeisl, J., Qu, Z.W., Zhu, H., Kroes, G.J., and Nørskov, J. (2007). Electrolysis of water on oxide surfaces. J. Electroanal. Chem. *607*, 83–89. https://doi.org/10.1016/j.jelechem.2006.11.008.

4. Man, I.C., Su, H.Y., Calle-Vallejo, F., Hansen, H.A., Martínez, J.I., Inoglu, N.G., Kitchin, J., Jaramillo, T.F., Nørskov, J.K., and Rossmeisl, J. (2011). Universality in oxygen evolution electrocatalysis on oxide surfaces. ChemCatChem *3*, 1159–1165. https://doi.org/10.1002/cctc.201000397.

5. Grimaud, A., Hong, W.T., Shao-Horn, Y., and Tarascon, J.M. (2016). Anionic redox processes for electrochemical devices. Nat. Mater. *15*, 121–126. https://doi.org/10.1038/nmat4551.

6. Mefford, J.T., Rong, X., Abakumov, A.M., Hardin, W.G., Dai, S., Kolpak, A.M., Johnston, K.P., and Stevenson, K.J. (2016). Water electrolysis on $La_{1-x}Sr_xCoO_{3-\delta}$ perovskite electrocatalysts. Nat. Commun. *7*, 11053. https://doi.org/10.1038/ncomms11053.

7. Mueller, D.N., Machala, M.L., Bluhm, H., and Chueh, W.C. (2015). Redox activity of surface oxygen anions in oxygen-deficient perovskite oxides during electrochemical reactions. Nat. Commun. *6*, 6097. https://doi.org/10.1038/ncomms7097.

8. Grimaud, A., Diaz-Morales, O., Han, B., Hong, W.T., Lee, Y.L., Giordano, L., Stoerzinger, K.A., Koper, M.T.M., and Shao-Horn, Y. (2018). Activate lattice oxygen redox reactions in metal oxides to catalyse oxygen evolution. Nat. Chem. *10*, 242. https://doi.org/10.1038/nchem.2932.

9. Sun, Y., Liao, H., Wang, J., Chen, B., Sun, S., Ong, S.J.H., Xi, S., Diao, C., Du, Y., Wang, J.O., et al. (2020). Covalency competition dominates the water oxidation structure-activity relationship on spinel oxides. Nat. Catal. *3*, 959. https://doi.org/10.1038/s41929-020-00548-z.

10. Pan, Y., Xu, X., Zhong, Y., Ge, L., Chen, Y., Veder, J.P.M., Guan, D., O'Hayre, R., Li, M., Wang, G., et al. (2020). Direct evidence of boosted oxygen evolution over perovskite by enhanced lattice oxygen participation. Nat. Commun. *11*, 2002. https://doi.org/10.1038/s41467-020-15873-x.

11. Song, J., Wei, C., Huang, Z.F., Liu, C., Zeng, L., Wang, X., and Xu, Z.J. (2020). A review on fundamentals for designing oxygen evolution electrocatalysts. Chem. Soc. Rev. *49*, 2196–2214. https://doi.org/10.1039/c9cs00607a.

12. Huang, Z.F., Lin, B.Q., Torsha, T.T., Dilshad, S., Yang, D.S., Xiao, J., Wang, C., Xu, Z.C.J., and Wang, X. (2019). Chemical and structural origin of lattice oxygen oxidation in Co-Zn oxyhydroxide oxygen evolution electrocatalysts. Nat. Energy *32*, 329–337. https://doi.org/10.1038/s41560-019-0355-9.

13. Wang, C., Zhang, Q., Yan, B., You, B., Zheng, J., Feng, L., Zhang, C., Jiang, S., Chen, W., and He, S. (2023). Facet engineering of advanced electrocatalysts toward hydrogen/oxygen evolution reactions. Nano-Micro Lett. *15*, 52. https://doi.org/10.1007/s40820-023-01024-6.

14. Du, C., Li, P., Zhuang, Z., Fang, Z., He, S., Feng, L., and Chen, W. (2022). Highly porous nanostructures: rational fabrication and promising application in energy electrocatalysis. Coord. Chem. Rev. *466*, 214604. https://doi.org/10.1016/j.ccr.2022.214604.

15. Wang, C., Yan, B., Chen, Z., You, B., Liao, T., Zhang, Q., Lu, Y., Jiang, S., and He, S. (2021). Recent advances in carbon substrate supported nonprecious nanoarrays for electrocatalytic oxygen evolution. J. Mater. Chem. A Mater. *9*, 25773–25795. https://doi.org/10.1039/d1ta08039c.

16. Wang, X., Xi, S., Huang, P., Du, Y., Zhong, H., Wang, Q., Borgna, A., Zhang, Y.W., Wang, Z., Wang, H., et al. (2022). Pivotal role of reversible NiO_6 geometric conversion in oxygen evolution. Nature *611*, 702–708. https://doi.org/10.1038/s41586-022-05296-7.

17. Krukau, A.V., Vydrov, O.A., Izmaylov, A.F., and Scuseria, G.E. (2006). Influence of the exchange screening parameter on the performance of screened hybrid functionals. J. Chem. Phys. *125*, 224106. https://doi.org/10.1063/1.2404663.

18. Heyd, J., Scuseria, G.E., and Ernzerhof, M. (2003). Hybrid functionals based on a screened Coulomb potential. J. Chem. Phys. *118*, 8207–8215. https://doi.org/10.1063/1.1564060.

19. Lægsgaard, J., and Stokbro, K. (2001). Hole trapping at Al impurities in silica: a challenge for density functional theories. Phys. Rev. Lett. *86*, 2834–2837. https://doi.org/10.1103/PhysRevLett.86.2834.

20. Droghetti, A., Pemmaraju, C.D., and Sanvito, S. (2008). Predicting d_0 magnetism: self-interaction correction scheme. Phys. Rev. B *78*, 140404. https://doi.org/10.1103/PhysRevB.78.140404.

21. Deák, P., Aradi, B., and Frauenheim, T. (2011). Polaronic effects in TiO_2 calculated by the HSE06 hybrid functional: dopant passivation by carrier self-trapping. Phys. Rev. B *83*, 155207. https://doi.org/10.1103/PhysRevB.83.155207.

22. Franchini, C., Reticcioli, M., Setvin, M., and Diebold, U. (2022). Polarons in materials. Nat. Rev. Mater. *7*, 250. https://doi.org/10.1038/s41578-022-00424-1.

23. Tang, W., Sanville, E., and Henkelman, G. (2009). A grid-based Bader analysis algorithm without lattice bias. J. Phys. Condens. Matter *21*, 084204. https://doi.org/10.1088/0953-8984/21/8/084204.

24. Sanville, E., Kenny, S.D., Smith, R., and Henkelman, G. (2007). Improved grid-based algorithm for Bader charge allocation. J. Comput. Chem. *28*, 899–908. https://doi.org/10.1002/jcc.20575.

25. Schneider, J., Matsuoka, M., Takeuchi, M., Zhang, J., Horiuchi, Y., Anpo, M., and Bahnemann, D.W. (2014). Understanding TiO_2 photocatalysis: mechanisms and materials. Chem. Rev. *114*, 9919–9986. https://doi.org/10.1021/cr5001892.

26. Arroyo-de Dompablo, M.E., Morales-García, A., and Taravillo, M. (2011). DFT+*U* calculations of crystal lattice, electronic structure, and phase stability under pressure of TiO_2 polymorphs. J. Chem. Phys. *135*, 054503. https://doi.org/10.1063/1.3617244.

27. Wang, D., Wang, L., Chen, J.F., Wang, H.F., and Hu, P. (2018). Identifying the key obstacle in photocatalytic oxygen evolution on rutile TiO_2. Nature Catalysis *19*, 291–299. https://doi.org/10.1038/s41929-018-0055-z.

28. Koper, M.T.M. (2013). Theory of multiple proton-electron transfer reactions and its implications for electrocatalysis. Chem. Sci. *4*, 2710–2723. https://doi.org/10.1039/c3sc50205h.

29. Giordano, L., Han, B., Risch, M., Hong, W.T., Rao, R.R., Stoerzinger, K.A., and Shao-Horn, Y. (2016). pH dependence of OER activity of oxides: current and future perspectives. Catal. Today *262*, 2–10. https://doi.org/10.1016/j.cattod.2015.10.006.

30. Chen, X., Choing, S.N., Aschaffenburg, D.J., Pemmaraju, C.D., Prendergast, D., and Cuk, T. (2017). The Formation time of Ti–$O^{\cdot}$ and Ti–$O^{\cdot}$–Ti radicals at the n-$SrTiO_3$/aqueous interface during photocatalytic water oxidation. J. Am. Chem. Soc. *139*, 1830–1841. https://doi.org/10.1021/jacs.6b09550.

31. Kresse, G., and Hafner, J. (1993). Ab initio molecular dynamics for liquid metals. Phys. Rev. B *47*, 558–561. https://doi.org/10.1103/physrevb.47.558.

32. Kresse, G., and Hafner, J. (1994). Ab initio molecular-dynamics simulation of the liquid-metal–amorphous-semiconductor transition in germanium. Phys. Rev. B *49*, 14251–14269. https://doi.org/10.1103/physrevb.49.14251.

33. Kresse, G., and Furthmüller, J. (1996). Efficiency of ab-initio total energy calculations for metals and semiconductors using a plane-wave basis set. Comput. Mater. Sci. *6*, 15–50. https://doi.org/10.1016/0927-0256(96)00008-0.

34. Kresse, G., and Joubert, D. (1999). From ultrasoft pseudopotentials to the projector augmented-wave method. Phys. Rev. B *59*, 1758–1775. https://doi.org/10.1103/PhysRevB.59.1758.

35. Wei, S.H. (2004). Overcoming the doping bottleneck in semiconductors. Comput. Mater. Sci. *30*, 337–348. https://doi.org/10.1016/j.commatsci.2004.02.024.

36. Xu, H., Zhang, R.Q., Ng, A.M.C., Djurišić, A.B., Chan, H.T., Chan, W.K., and Tong, S.Y. (2011). Splitting water on metal oxide surfaces. J. Phys. Chem. C *115*, 19710–19715. https://doi.org/10.1021/jp2032884.

STAR★METHODS

KEY RESOURCES TABLE

REAGENT or RESOURCE	SOURCE	IDENTIFIER
Software and algorithms		
VASP	G. Kresse et al.	https://www.vasp.at/
VESTA	Koichi et al.	http://jp-minerals.org/vesta/en/

RESOURCE AVAILABILITY

Lead contact

Further information and requests for resources and reagents should be directed to and will be fulfilled by the lead contact, Shuk-Yin Tong (tongsy@cuhk.edu.cn).

Materials availability

This study did not generate new unique reagents.

Data and code availability

- All data reported in this paper will be shared by the lead contact upon request
- This paper does not report original code.
- Any additional information required to reanalyze the data reported in this paper is available from the lead contact upon request

METHOD DETAILS

(a) We perform spin-polarized DFT calculations with HSE06 functionals[17,18,31–33] because the Hamiltonian describes better the polaronic hole within the O p shell.[19–21] The electron-ion interaction is described by the projected augmented wave (PAW) method[34] with $3d^2 4s^2$ and $2s^2 2p^4$ treated as valence states for Ti and O, respectively. The rutile TiO_2 (110) slab is modeled using a (4×2) two-dimensional supercell with four Ti layers and rectangular surface cell of 11.808 × 13.013 $Å^2$. There are 64 Ti atoms and 128 lattice O atoms in the slab. The slabs are separated by a ~12 Å vacuum. We use a plane wave cutoff energy of 450 eV, and k sampling is restricted to the Γ point. The structures are fully relaxed at each step with forces converged to $\leq$ 0.05 eV/Å on each atom. Charge removal from the system is by the jellium method.[35] The 4e removal steps involve the adsorption of two water molecules. Previous work[36] have shown that water adsorbs molecularly at the Ti_5 site.

(b) The charge of oxygen and hydrogen in water: The neutral oxygen atom carries 6e ($2s^2 2p^4$) in its valence band. In a water molecule, DFT calculates that each hydrogen gives 0.62e to oxygen (ionicity = 62.0%), resulting in each O_w carrying 7.24e while each H carrying 0.38e.

(c) The charge of titanium and lattice oxygen in the TiO_2 (110) slab: The neutral Ti atom carries 4e ($3d^2 4s^2$) in its valence band. In the TiO_2 (110) slab, DFT calculates that each bulk Ti atom gives a total of 2.1e to its six lattice oxygen neighbors (ionicity = 52.5%), resulting in each Ti carrying an average charge of 1.9e. Each bulk lattice O atom receives a total of 1.05e from its three Ti neighbors, resulting in each O carrying an average charge of 7.05e. The actual amount of charge carried by each atom in the slab varies and is shown in the charge distribution tables (supplementary information).

(d) Charge flow at metal atoms in pathway 1: On TiO_2 (110), where the metal bands are well below the Fermi level, there is little charge movement into or out of metal atoms in the four steps. For example, the 5-fold surface metal atom Ti_5 carries 1.92e before water adsorption (Figure 2 upper panel, the IS state). Upon water adsorption with the formation of an OH dimer on Ti_5 (the S1 state),the charge on Ti_5 becomes 1.88e. Thus, only 0.04e has flowed out of the anchoring metal atom, a totally insignificant amount.